Journal of Power Sources, 29 (1990) 321 - 332

THE ELECTROCHEMICAL GENERATION OF USEFUL CHEMICAL SPECIES FROM LUNAR MATERIALS

KAN J. TSAI, DANIEL J. KUCHYNKA and ANTHONY F. SAMMELLS*
Eltron Research, Inc., Aurora, IL 60504 (U.S.A.)

Summary

Electrochemical cells have been fabricated for the simultaneous generation of oxygen and lithium from an Li_2O-containing molten salt (Li_2O–LiCl–LiF). The cell utilizes an oxygen vacancy conducting solid electrolyte, yttria-stabilized zirconia (YSZ), to effect separation between oxygen evolving and lithium reduction half-cell reactions. The cell, which operates at 700 - 850 °C, possesses rapid electrode kinetics at the lithium-alloy electrode with exchange current density (i_o) values being >60 mA cm^{-2}. When used in the electrolytic mode, lithium produced at the negative electrode would be continuously removed from the cell for later use (under lunar conditions) as an easily storable reducing agent (compared with H_2) for the chemical refining of lunar ores. Because of the high reversibility of this electrochemical system, it has also formed the basis for the lithium–oxygen secondary battery system which possesses the highest theoretical energy density yet investigated.

Introduction

The strategy being pursued for lunar ore refining is based upon electrochemical cells possessing the general configuration:

Li alloy/Li_2O–LiCl–LiF molten salt/YSZ/$La_{0.89}Sr_{0.11}MnO_3$

In practical electrolytic cells, lithium produced at the negative electrode would, after removal from the cell, be available for lunar ore refining via the general chemical reaction:

$$2Li + MO \longrightarrow Li_2O + M$$

where MO represents a lunar ore. Emphasis to this time has been on Fe_2O_3, TiO_2 and the lunar ore ilmenite ($FeTiO_3$), all of which have been shown to be chemically reducible by Li to give metals. The resulting Li_2O reaction product could then be removed from the solid-state reaction mixture by sublimation and reintroduced into the negative electrode compartment of

*Author to whom correspondence should be addressed.

0378-7753/90/$3.50

the electrolytic cell to be electrolyzed again. Hence, this electrochemical approach provides a convenient route for the simultaneous generation of both metals and oxygen from lunar materials on the Moon's surface. It has previously been suggested that oxygen might be extracted from ilmenite by its initial chemical reduction by hydrogen, initially transported from Earth [1 - 3], and presumably requiring cryogenic storage on the Moon's surface. Other approaches discussed for the chemical reduction of lunar ores have included carbothermic reduction to give the desired metal [4, 5]. Previous work by others has also investigated the direct high temperature electrochemistry of simulated lunar materials (molten silicates), using platinum electrodes. Electrolysis of these melts demonstrated simultaneous oxygen evolution at the anode [6 - 10] and deposition of an impure metal–silicon alloy slag at the cathode [11 - 14]. Nevertheless, this preliminary work showed feasibility for high temperature molten salt electrochemistry as an attractive approach for oxygen evolution and metal reduction from lunar type ores. In the approach being discussed here, oxygen evolution and lunar ore reduction are separated into distinct electrochemical and chemical steps. This strategy minimizes the opportunity of lunar-ore-originating-impurities entering the electrochemical cell and degrading performance.

The reducing power of lithium is significantly greater than that of hydrogen. This fact can be summarized by the two general reactions:

$$H_2 + \tfrac{1}{2}O_2 \longrightarrow H_2O \qquad \Delta G = -68 \text{ kcal mole}^{-1} \text{ (25 °C)} \tag{1}$$

and

$$2Li + \tfrac{1}{2}O_2 \longrightarrow Li_2O \qquad \Delta G = -142 \text{ kcal mole}^{-1} \text{ (25 °C)} \tag{2}$$

The corresponding free energy of reaction between lithium and candidate metal oxides of interest at 1000 K are summarized in Table 1.

TABLE 1

Free energy of reaction between lithium and metal oxides at 1000 K

	ΔG (kcal mole^{-1})
$4Li + SiO_2 \rightarrow 2Li_2O + Si$	−28.0
$2Li + FeO \rightarrow Li_2O + Fe$	−53.9
$4Li + TiO_2 \rightarrow 2Li_2O + Ti$	−15.6
$6Li + Cr_2O_3 \rightarrow 3Li_2O + 2Cr$	−87.9

We estimate the free energy change associated with ilmenite reduction by lithium at 1000 K, corresponding to the overall reaction:

$$FeTiO_3 + 6Li \longrightarrow Fe + Ti + 3Li_2O \tag{3}$$

to be $\Delta G = -62.2$ kcal mole^{-1}. Hence, lithium would appear to be a sufficiently strong reducing agent for many of the transition metal oxides anticipated to be present on the Moon's surface.

The electrochemistry occurring in these cells possesses high reversibility, and consequently has given us the opportunity to study the lithium/oxygen secondary battery. The overall electrochemistry occurring in this cell upon discharge/charge cycling can be represented by:

$$FeSi_2Li_x + \tfrac{1}{2}O_2(air) \underset{\text{charge}}{\overset{\text{discharge}}{\rightleftharpoons}} Li_2O \text{ (in molten salt)} + FeSi_2 \quad (4)$$

with overall capacity being dictated by the concentration of Li_2O that may be incorporated within the negative electrode compartment of this electrochemical cell. Although theoretical energy densities for a given battery system are often a poor indicator of the final practical energy density that might be achieved, it is of interest to note that the energy density for electroactive materials in the lithium–oxygen system calculates to 4082 W h kg^{-1} compared with 2211 W h kg^{-1} for the lithium–chlorine cell; the highest energy density secondary system investigated to this time. The significant technical observations to be discussed which make this an attractive secondary battery system are:

(i) both electrodes possess high electrochemical reversibility;

(ii) the anodic reaction upon cell charge involves the exclusive evolution of oxygen;

(iii) a significant concentration of Li_2O can be incorporated into the Li_2O–LiCl–LiF ternary melt.

A comparison of the lithium–oxygen secondary cell with other major conventions and advanced systems is shown in Table 2.

TABLE 2

Major secondary batteries for electrical energy storage by comparison with the lithium–oxygen system

Battery system	Negative	Positive	OCP (V)	Theoretical energy density for electroactive matls. (W h kg^{-1})
Lead–acid	Pb	PbO_2	2.0	238
Nickel–cadmium	Cd	NiOOH	1.2	148
Nickel–zinc	Zn	NiOOH	1.7	448
Zinc–chlorine	Zn	Cl_2	2.12	829
Lithium–iron sulfide	Li(Al)	FeS	1.2	626
Sodium–sulfur	Na	S	2.1	760
Lithium–chlorine	Li	Cl_2	3.53	2211
Lithium–oxygen	Li	O_2	2.3	4082

Results and discussion

Previous work performed in our laboratory [15] showed that the ternary molten salt system Li_2O–LiF–LiCl is an attractive candidate elec-

trolyte for this electrochemical cell. The utility of this molten salt electrolyte was dependent, however, upon gaining some insight into the amount of Li_2O that could be accommodated in the LiF–LiCl (70 mol%) molten salt and its impact upon the resulting solid–liquidus curve. This was performed by progressively introducing Li_2O in 2 - 5 mol% increments into an LiF–LiCl (70 mol%) binary mixture in a conventional conductivity-type cell. After each Li_2O addition, the ternary molten salt mixture was initially heated to 550 °C, at which temperature it became molten. The resulting molten salt ionic conductivity values were measured between stainless steel electrodes (1 cm^2) placed 1.5 cm apart during slow cell cooling so as to minimize interelectrode thermal gradients. The molten salt freezing point was detected by a dramatic decrease in measured ionic conductivity. The resulting solid–liquidus curve obtained for this ternary system is shown in Fig. 1, which indicates that for Li_2O contents above ≅18 mol% the molten salt goes into a two-phase region consisting of Li_2O (18 mol%), LiF (24.6 mol%), LiCl (57.4 mol%) in direct contact with solid Li_2O. The important point here is that excess Li_2O could be introduced into the electrolyte cell and would not promote melt freezing.

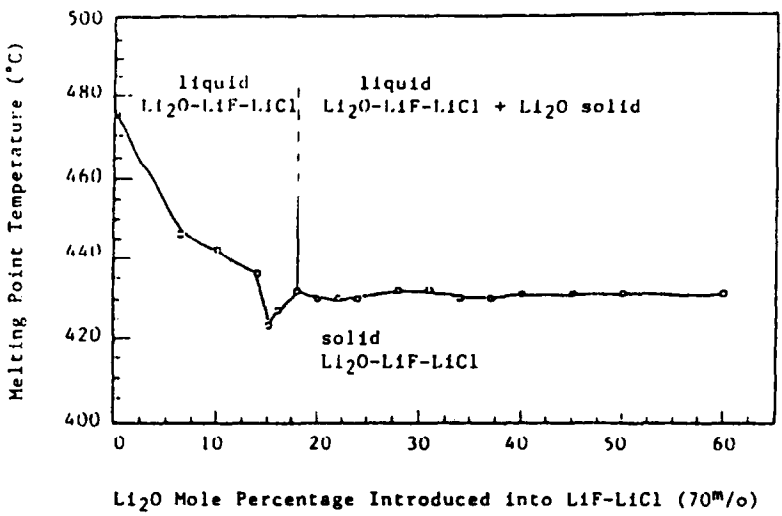

Fig. 1. Solid–liquidus curve for Li_2O–LiF–LiCl molten salt as a function of Li_2O.

Both half and full cell electrochemical measurements have been performed on this cell. Coulometric lithium deposition has been performed on both iron and iron silicide ($FeSi_2$) negative electrode substrates. Iron silicide was of interest since lithium deposition results in the formation of a series of distinct electrochemically reversible lithium compounds up to the composition $FeSi_2Li_{10}$. This has not only permitted us to store lithium conveniently in the negative electrode compartment of the reversible lithium–oxygen storage battery, but also acts as a substrate for wetting lithium, facilitating its later removal from the negative electrode compartment of the

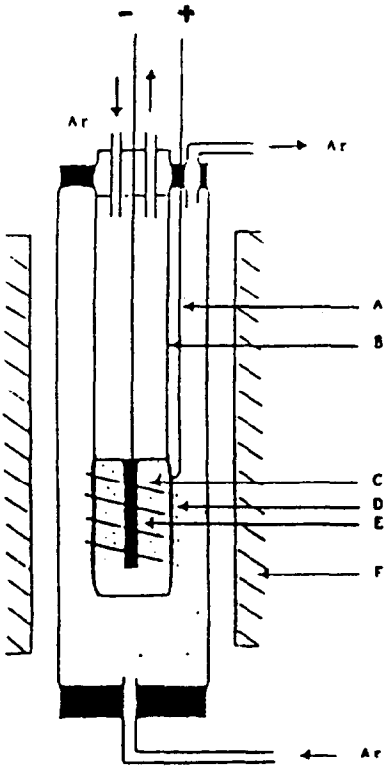

Fig. 2. Schematic drawing of cell configuration used for the simultaneous electrolytic generation of lithium and oxygen. A, Anode current collector; B, calcia or yttria stabilized zirconia; C, molten salt; D, $La_{0.89}Sr_{0.11}MnO_3$ anode; E, stainless steel or $FeSi_2$ cathode; F, furnace.

electrolytic cell. Preliminary current–potential characteristics of this electrode were performed in electrolytic cells possessing the general configuration shown in Fig. 2. The charging current–potential curves for this cell (Fig. 3) clearly show voltage plateaux associated with each ternary lithium compound. Electrode kinetics for this electrode were performed using a molten salt of composition Li_2O (6.4 mol%), LiF(28.1 mol%), LiCl(65.5 mol%) using $FeSi_2Li_x$ for the working-, and $SiLi_4$ for counter and reference electrodes. For voltage plateaux corresponding to the respective ternary alloys $FeSi_2Li_6$, $FeSi_2Li_8$ and $FeSi_2Li_{10}$, cyclic voltammetry scans (50 mV s^{-1}) were performed ±200 mV from its initial open circuit potential (OCP) with respect to the $SiLi_4$ reference. A representative current–overpotential curve is shown in Fig. 4, which was analyzed by use of the Allen–Hickling relationship:

$$\log \frac{i}{\exp(\alpha\eta F/RT)^{-1}} = \log i_o - \frac{\alpha\eta F}{2.303RT} \tag{5}$$

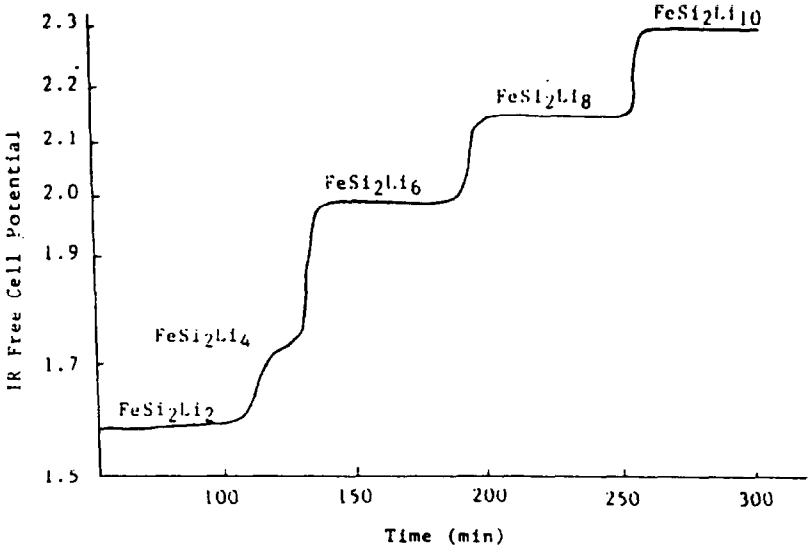

Fig. 3. *IR* free charge curve for $FeSi_2$ in 28.5 mol% LiF, 66.5 mol% LiCl and 5 mol% Li_2O at 650 °C *vs.* $La_{0.89}Sr_{0.11}MnO_3$/Pt (air). Current density 10 mA cm^{-2}.

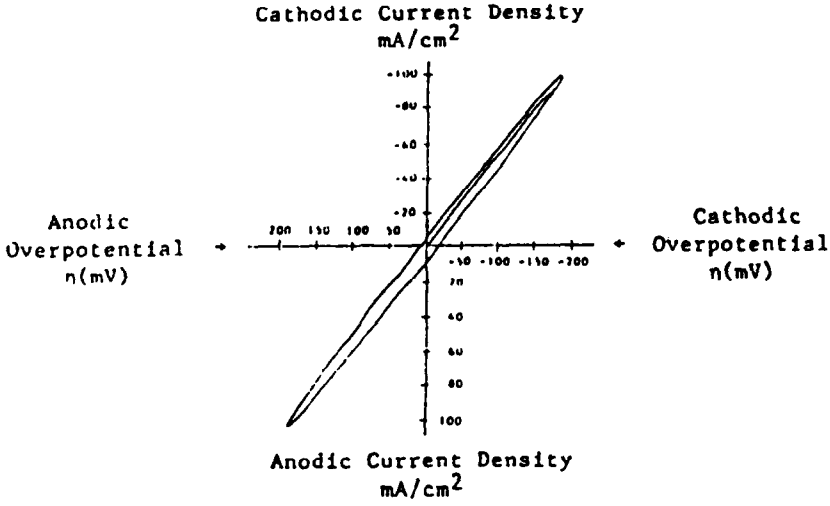

Fig. 4. Current–overpotential curve for the cell $FeSi_2Li_{10}/Li_2O$–LiF–LiCl/$SiLi_4$ at 800 °C. Initial open circuit potential —71 mV with respect to $SiLi_4$ reference. Scan rate 50 mV s^{-1}.

where i_o was the exchange current density from which a direct estimation of relative electrode kinetics was determined, η was the electrode overpotential, α the transfer coefficient, and the other symbols had their usual significance [16]. Exchange current densities (i_o) were obtained from the intercept by plotting η *versus* log $i/\exp(\alpha\eta F/RT)^{-1}$. The dependency of i_o upon both cell temperature and lithium alloy composition is summarized in Table 3. These

TABLE 3

Dependence of exchange current density on both cell temperature and lithium alloy composition

Cell temperature (°C)	Measured exchange $FeSi_2Li_{10}$	Current density $FeSi_2Li_8$	i_o (mA cm^{-2}) $FeSi_2Li_6$
650	49.7	50.6	43.7
700	54.5	54.7	50.9
750	56.0	57.2	55.6
800	64.5	65.7	58.2

current–voltage measurements clearly showed the presence of rapid electrode kinetics at the negative electrode, suggesting that this Faradaic process will not be the rate limiting process in the finally developed electrochemical cell.

In fully developed electrolytic cells we must facilitate the convenient removal of faradaically deposited lithium at the negative electrode. One of the major obstacles to achieve this is related to the high surface tension of Li at 700 °C (320 dynes cm^{-1}) which compares with Hg (400 dynes cm^{-1}) at room temperature. Deposited lithium resident in a porous electrode structure, in the absence of wetting, can, as a consequence, prove difficult to remove physically via a proximate orifice. We have found, however, that both $SiLi_x$ and $FeSi_2Li_x$ can act as effective substrate sites for wetting faradaically deposited lithium, thereby providing a strategy for the subsequent continuous removal of lithium from the electrolytic cell. A schematic of the experimental arrangement used for comparing approaches for lithium removal is shown in Fig. 5. Lithium could be conveniently removed from the cell by application of ≅5 psi into the lithium chamber, C, thereby enabling its transfer into glass trap, D. In the event of lithium/molten salt mixtures being formed in the electrochemical cell, we have found that effective segregation into two distinct phases can be achieved if the stainless steel transfer tube between the electrolytic cell and lithium storage compartment is initially silicided to form a thin coating of $FeSi_2$. Subsequent reaction of this thin coating with lithium to give $FeSi_2Li_x$ will provide the necessary wetting characteristic necessary for promoting preferential lithium migration from the electrolytic cell.

As we have previously discussed, lithium is a strong reducing agent which should, in principle, be able to reduce simulated lunar ores to the corresponding metal. This has been examined by investigating direct reaction between lithium and the respective metal oxides TiO_2, Fe_2O_3 and $FeTiO_3$. Here, thermal analyses were performed under both argon and vacuum (≈100 μm). Lithium and the metal oxide of interest were initially placed into a small boron nitride crucible located inside a 3/4 in. Swagelock union used as the reaction chamber. A chromel–alumel thermocouple was placed in direct contact with the reaction mixture. Because of the anticipated high reducing ability of lithium, only 0.02 g was used for each reaction, with an excess of

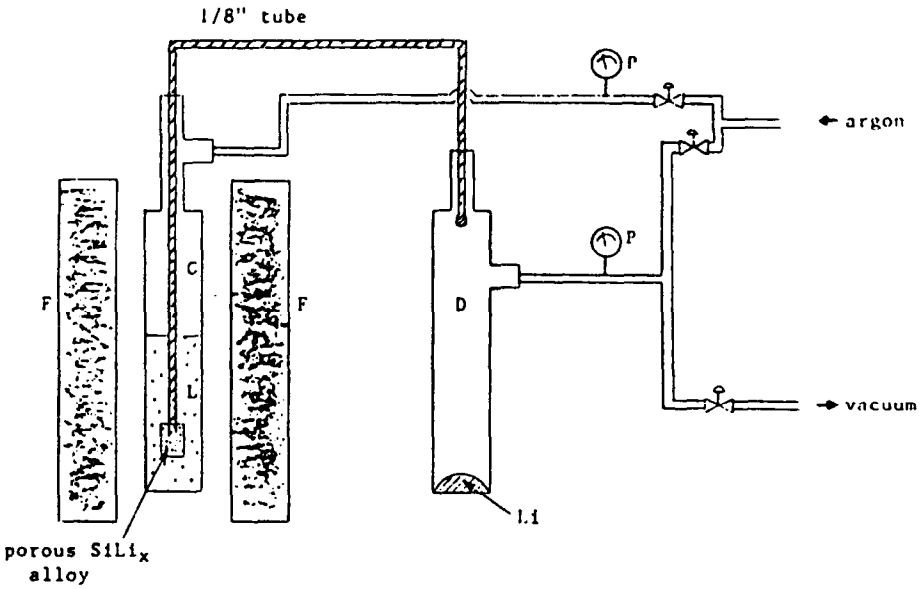

Fig. 5. Schematic diagram for simulated lithium removal process. C, lithium containing chamber; D, lithium collecting chamber; F, furnace; L, lithium; P, pressure gauge.

metal oxide being present. The reaction chamber was heated at 5 °C min^{-1}. The inception of solid-state reaction was manifested by a rapid temperature increase in all cases investigated, indicating the reaction to be highly exothermic and irreversible. Thermal analyses for, respectively, Fe_2O_3 and TiO_2 are shown in Fig. 6(A) and (B). The reaction product between Li and Fe_2O_3 was clearly shown to be elemental iron which could be conveniently removed with a magnet. Analysis of the reaction mixture between Li and TiO_2 was determined by initially dissolving with 37 wt.% HCl. Here, unreacted TiO_2 was insoluble, whereas Ti dissolved as $TiCl_3$ to give a dark-blue solution. Quantitative determination of elemental Ti was then performed spectrophotometrically. Based upon the initial Li present in the reaction mixture, approximately 80% participated in promoting TiO_2 reduction to Ti. Tem-

TABLE 4

Experimentally observed temperatures and heat of reaction for the inception of reaction between lithium and the metal oxide of interest

Metal oxide	Temperature for inception of solid-state reaction (°C)	Heat of reaction (kcal $mole^{-1}$) calc'd at temperature
TiO_2	457	−71.6
Fe_2O_3	440	−244.8
$FeTiO_3$ (ilmenite)	432	—
$Fe_2O_3 + TiO_2$ (1:1)	428	−157.2

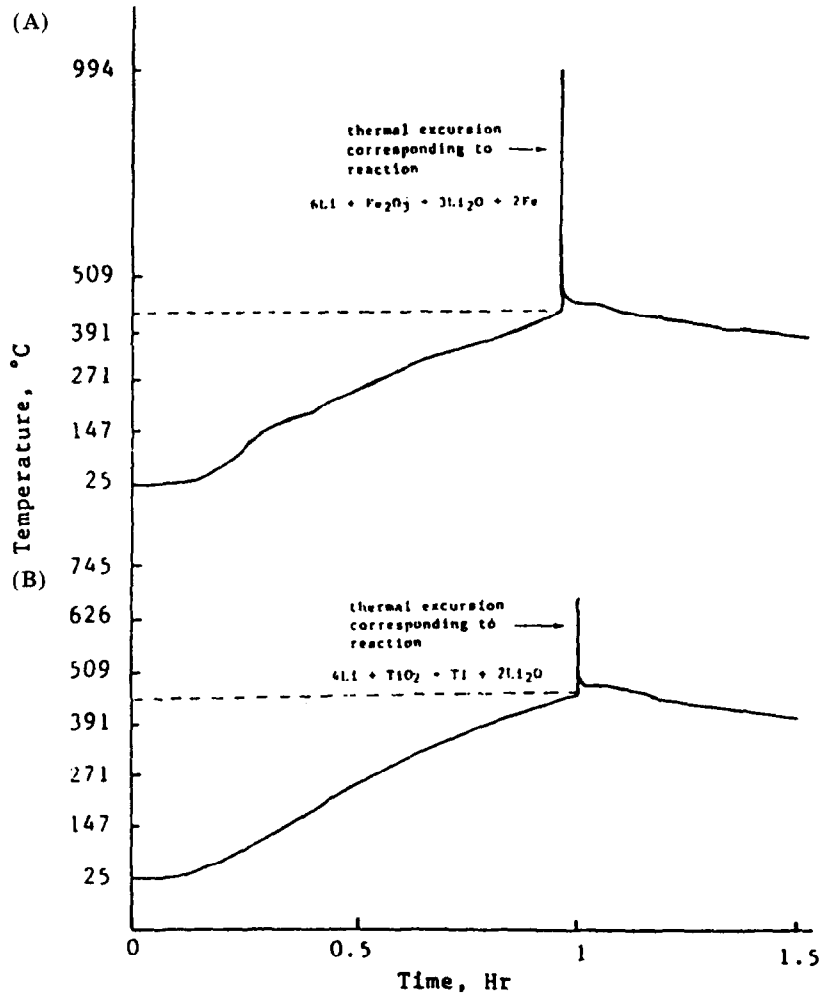

Fig. 6. Thermal analysis for detection of solid-state reaction temperature (A) between Li and Fe_2O_3 (excess); (B), TiO_2 (excess) under argon.

peratures experimentally observed for the inception of these reactions are summarized in Table 4, together with the corresponding calculated heat of reaction at each respective temperature.

This electrochemical technology, as we have already discussed, is also compatible for a high energy secondary battery. Initial work [17] towards this goal focussed upon electrochemical cell configurations analogous to that shown in Fig. 2, where maintenance of an inert (Ar) atmosphere in the negative electrode component could be conveniently achieved [18]. A preliminary charge–discharge curve for this type of cell using an $FeSi_2Li_x$ negative electrode is shown in Fig. 7. Again, the voltage plateaux observed correspond to the reversible formation of ferrosilicon–lithium alloys.

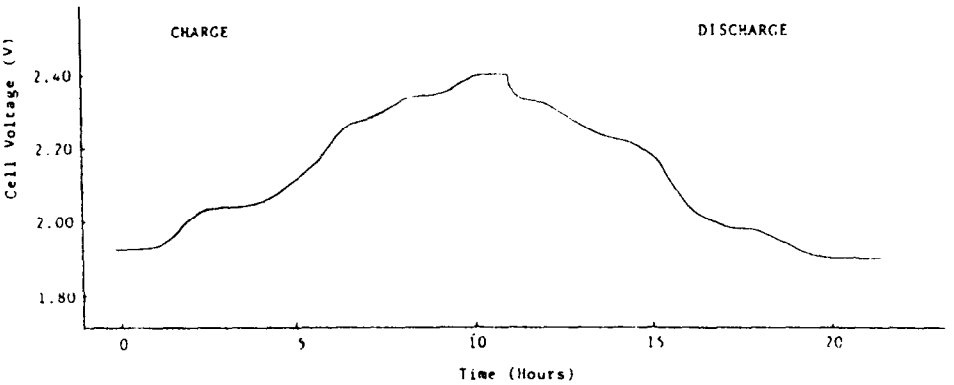

Fig. 7. *IR*-free charge–discharge curve for the cell Li_xFeSi_2/(52.5–23.6–23.9) mol.% LiCl–LiF–Li_2O/ZrO_2 (5 wt.% CaO)/$La_{0.89}Sr_{0.11}MnO_3$/Pt at 20 mA cm^{-2} (at negative electrode). Total cell resistance 24 Ω. Temperature 650 °C.

Furthermore, it was found during cell charge that the volume of oxygen generated was, in fact, Faradaic, demonstrating that even in direct contact with halide containing molten salt, the solid electrolyte remains an exclusive oxygen anion conductor.

For practical reversible lithium/oxygen batteries for terrestrial applications, however, we must identify a design which will enable us to operate in

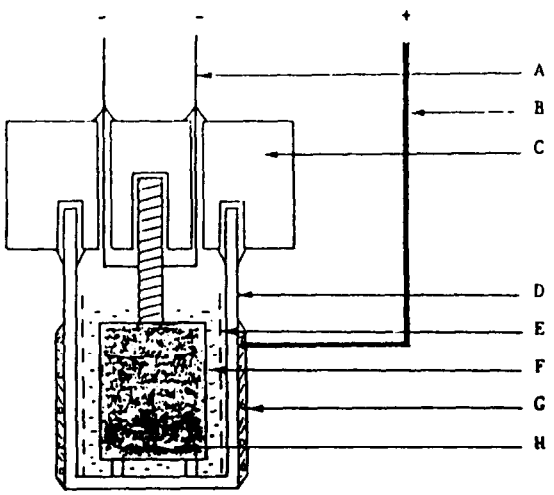

Fig. 8. Schematic design of the lithium/oxygen secondary storage cell discussed in the text. A, Current collector nickel–chromium (80:20) (—); B, platinum current collector (+) tightly wound around YSZ crucible; C, machined alumina cap; D, YSZ O^{2-} conducting solid electrolyte; E, zirconia felt separator; F, molten salt containing 66.5 mol% LiCl, 28.5 mol% LiF and 5 mol% Li_2O; G, $La_{0.89}Sr_{0.11}MnO_3$ electrocatalyst; H, $FeSi_2$-Li_8 negative electrode.

the atmosphere. This has been addressed by fabrication of small prototype cells possessing the general design shown in Fig. 8. The design is based upon a 5 cm high YSZ crucible possessing respective inside and outside diameters of 2.1 and 2.35 cm (total volume 19 ml). Cells were fabricated in the partially-charged state using $FeSi_2Li_8$ as the negative electroactive material. Current collection from this electrode was via an aluminized nickel–chromium alloy (Ni (76%), Cr (16%), Al (4.5%), Fe (3%), Y (trace), Haynes Alloy 214). The $La_{0.89}Sr_{0.11}MnO_3$ oxygen electrode was initially prepared [19] from a 15 wt.% suspension, in poly(vinyl alcohol)–ethylene glycol, of the appropriate stoichiometric metal nitrates. Current collection from this region was via a Pt wire initially tightly coiled in this area. Synthesis of the perovskite electrocatalyst was achieved by heating in the atmosphere to ≅1000 °C for 1 h. Protection of the negative electrode compartment from direct contact with the atmosphere was achieved using a machined alumina cover (Cotronics, Inc.) whose residual porosity was removed by use of a coating of high density ceramic cement (Sauereisen #8), followed by curing at 90 °C for one day.

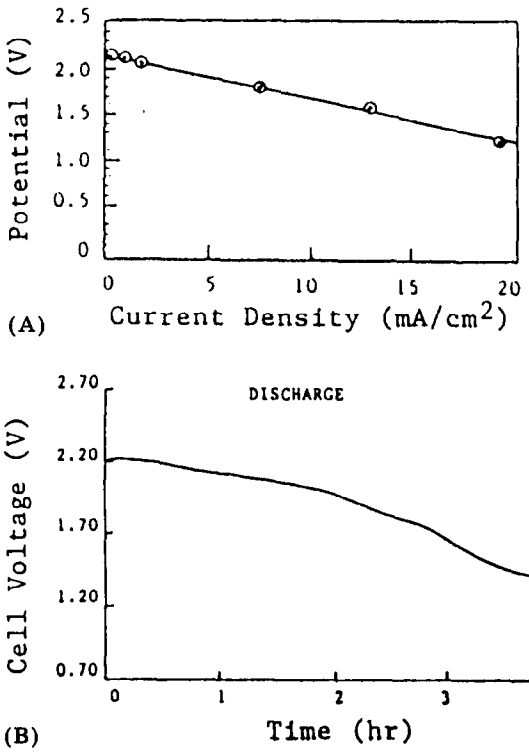

Fig. 9. Current–potential and discharge curves for the lithium/oxygen cell at A, 800 °C (R_{cell} = 3.9 Ω); B, 850 °C at a $C/50$ rate (5.3 mA cm^{-2}).

In partially charged cells fabricated here, the negative electrode compartment initially contained a molten salt of composition LiCl (66.5 mol%), LiF (28.5 mol%), Li_2O 5 mol%). This cell was operated in the atmosphere by initially heating to 600 °C, at which temperature the open-circuit potential became 2.2 V. Between 650 °C and 800 °C the overall cell resistance decreased from 47 Ω to 3.9 Ω. This reflected the improved O^{2-} conductivity for the solid electrolyte at higher temperatures. E_a was found to be 16 kcal $mole^{-1}$, similar to literature values [20]. Current–potential and discharge curves for this cell are shown in Fig. 9 (A) and (B).

The above discussed results demonstrate that this electrochemical technology is evolving into a practical option for both the generation of chemical species on the Moon's surface and as a high energy secondary battery for either terrestrial or lunar applications.

Acknowledgement

This work was supported by NASA Johnson Space Center under Contract No. NAS9-17991.

References

1 H. P. Davis, *Eagle Engin. Rep. #EE1 83-63*, Houston, 1983.
2 M. A. Gibson and C. W. Knudsen, in *Lunar Bases and Space Activities of the 21st Century*, NASA, 1984, p. 26.
3 E. Kibler, L. W. Taylor and R. J. Williams, in *Lunar Bases and Space Activities of the 21st Century*, NASA, 1984, p. 25.
4 W. C. Phinney *et al.*, in *Space-based Manufacturing from Nonterrestrial Materials*, Am. Inst. Aeronautics and Astronautics, New York, 1977.
5 A. H. Cutler in *Lunar Bases and Space Activities of the 21st Century*, NASA, 1984, p. 22.
6 K. W. Semkow and L. A. Haskin, *Geochim. Cosmochim. Acta, 49* (1985) 1897.
7 K. W. Semkow and L. A. Haskin, *Abstr. to Lunar Planet Sci., XVI* (1985) 761.
8 A. Ghosh and T. B. King, *Trans. Metall. Soc. AIME, 245* (1969) 145.
9 J. K. Higgins, *Glass Technol., 23* (1982) 90.
10 J. K. Higgins, *Glass Technol., 23* (1982) 180.
11 D. S. Kesterke, *U.S. Dept. of Interior Bur. Mines Rep. Invest. RI-7587*, 1971.
12 D. J. Lindstrom and L. A. Haskin, in T. Grey and C. Krop (eds.), *Space Manufacturing Facilities 3*, Am. Inst. Aeronautics and Astronautics, New York, 1979.
13 W. F. Carroll, *J. P. L. Rep. 83-36*, 1983.
14 R. H. Lewis, D. J. Lindstrom and L. A. Haskin, *Abstr. to Lunar Planet Sci., XVI* (1985) 489.
15 A. F. Sammells and K. W. Semkov, *J. Power Sources, 22* (1988) 285.
16 P. A. Allen and A. Hickling, *Trans. Faraday Soc., 53* (1957) 1626.
17 K. W. Semkow and A. F. Sammells, *J. Electrochem. Soc., 134* (1987) 2084.
18 K. W. Semkow and A. F. Sammells, *J. Electrochem. Soc., 134* (1987) 2088.
19 H.-M. Zhang, Y. Teraoka and N. Yamazoe, *N. Chem. Lett.*, (1987) 665.
20 T. H. Etsell and S. N. Flengas, *Chem. Rev., 70* (1970) 339.